

Mutations in CmVPS41 controlling resistance to cucumber mosaic virus display specific subcellular localization

Núria Real ¹, Irene Villar ^{1,2}, Irene Serrano ^{3,†}, Cèlia Guiu-Aragonés¹ and Ana Montserrat Martín-Hernández ^{1,4,*}

- 1 Centre for Research in Agricultural Genomics (CRAG) CSIC-IRTA-UAB-UB, C/Vall Moronta, Edifici CRAG, Bellaterra (Cerdanyola del Vallés), 08193 Barcelona, Spain
- 2 Universidad de Zaragoza, Calle Pedro Cerbuna, 12, 50009 Zaragoza, Spain
- 3 Laboratoire des Interactions des Plantes et Microorganismes, CNRS, 31326 Toulouse, France
- 4 Institut de Recerca i Tecnologia Agroalimentàries (IRTA), Edifici CRAG, C/ Vall Moronta, Bellaterra (Cerdanyola del Vallés), 08193 Barcelona, Spain

*Author for correspondence: montse.martin@irta.es

†Present address: Albrecht-von-Haller-Institute for Plant Sciences, Georg-August-University Göttingen, 37077 Göttingen, Germany.

N.R., I.V., I.S., and C.G.-A. performed research. N.R. analyzed the data and A.M.M.-H. designed research and wrote the manuscript.

The author responsible for distribution of materials integral to the findings presented in this article in accordance with the policy described in the Instructions for Authors (<https://academic.oup.com/plphys/pages/General-Instructions>) is: Ana Montserrat Martín-Hernández (montse.martin@irta.es).

Abstract

Resistance to cucumber mosaic virus (CMV) in melon (*Cucumis melo* L.) has been described in several exotic accessions and is controlled by a recessive resistance gene, *cmv1*, that encodes a vacuolar protein sorting 41 (CmVPS41). *cmv1* prevents systemic infection by restricting the virus to the bundle sheath cells, preventing viral phloem entry. CmVPS41 from different resistant accessions carries two causal mutations, either a G85E change, found in Pat-81 and Freeman's cucumber, or L348R, found in PI161375, cultivar Songwhan Charmi (SC). Here, we analyzed the subcellular localization of CmVPS41 in *Nicotiana benthamiana* and found differential structures in resistant and susceptible accessions. Susceptible accessions showed nuclear and membrane spots and many transvacuolar strands, whereas the resistant accessions showed many intravacuolar invaginations. These specific structures colocalized with late endosomes. Artificial CmVPS41 carrying individual mutations causing resistance in the genetic background of CmVPS41 from the susceptible variety Piel de Sapo (PS) revealed that the structure most correlated with resistance was the absence of transvacuolar strands. Coexpression of CmVPS41 with viral movement proteins, the determinant of virulence, did not change these localizations; however, infiltration of CmVPS41 from either SC or PS accessions in CMV-infected *N. benthamiana* leaves showed a localization pattern closer to each other, with up to 30% cells showing some membrane spots in the CmVPS41SC and fewer transvacuolar strands (reduced from a mean of 4 to 1–2) with CmVPS41PS. Our results suggest that the distribution of CmVPS41PS in late endosomes includes transvacuolar strands that facilitate CMV infection and that CmVPS41 re-localizes during viral infection.

Introduction

When viruses enter the plant, they must replicate, move cell-to-cell generally through plasmodesmata, up to the veins, surrounded by the bundle sheath (BS) cells, and invade the phloem cells, namely vascular parenchyma (VP) cells and companion cells to finally invade the whole plant, producing

a systemic infection (Hipper et al., 2013). Since viruses have a small and compact genome, encoding only a few genes, they must request the participation of many host factors to complete their cycle. Mutations in those host factors develop a loss of susceptibility that can either limit or prevent viral infection, thus, becoming resistance genes that are recessively

inherited (Hashimoto et al., 2016). Therefore, understanding how viral proteins and virions interact with host factors is key to prevent viral diseases.

Cucumber mosaic virus (CMV) is a positive-sense RNA virus able to infect over 1,200 plant species, including members of three important crop families, Solanaceae, Cruciferae, and Cucurbitaceae (Edwardson and Christie, 1991). CMV genome has three genomic and two subgenomic RNAs that encode five viral proteins. CMV strains are divided in two subgroups, I (SG I) and II (SG II), which share 70% of their sequence and present differences in their serological and chemical properties (Roossinck, 2001). In melon (*Cucumis melo* L.), few sources of resistance to CMV have been identified (Karchi et al., 1975; Pascual et al., 2019; Martín-Hernández and Picó, 2021), among them the Korean cultivar “Songwhan Charmi,” PI 161375 (from now on SC). SC shows an oligogenic and recessive resistance (Karchi et al., 1975), with a major gene, *cmv1*, conferring resistance to strains of SG II (Essafi et al., 2009; Guiu-Aragonés et al., 2015), and at least two other quantitative trait loci which, together with *cmv1* confer resistance to SG I strains (Guiu-Aragonés et al., 2014). The resistance conferred by *cmv1* is manifested as a restriction to phloem entry, since in the plants carrying this gene, strains of SG II (such as CMV-LS) can replicate and move cell-to-cell in the mesophyll up to the BS cells but are restricted in these cells and cannot move to the phloem cells. However, strains of SG I (such as CMV-FNY) can overcome this restriction and invade the phloem (Guiu-Aragonés et al., 2016). The viral factor determining this ability is the movement protein (MP), since a viral clone from CMV-LS carrying the MP from FNY can invade the phloem of the plant carrying the gene *cmv1* (Guiu-Aragonés et al., 2015).

Map-based cloning in melon has demonstrated that *cmv1* encodes a vacuolar protein sorting 41 (CmVPS41; Giner et al., 2017), a protein involved in the intracellular vesicle transport of cargo proteins from the late Golgi to the vacuole as part of the “homotypic fusion and vacuole protein sorting” (HOPS) complex, both via endosomes and also through vesicles, via the AP-3 pathway (Balderhaar and Ungermann, 2013; Schoppe et al., 2020). HOPS is a complex of six subunits, four of them shared (VPS11, VPS33, VPS16, and VPS18) with CORVET, another complex involved in endosome life cycle. The remaining two, VPS39 and VPS41, are required for the tethering function, with VPS41 the effector subunit of HOPS promoting vacuole fusion (Price et al., 2000). VPS41 is localized in late endosomes in *Arabidopsis* (*Arabidopsis thaliana*; Brillada et al., 2018). In yeast (*Saccharomyces cerevisiae*), VPS41p participates in the membrane fusion of cargo proteins between late endosomes and lysosomes (Rehling et al., 1999). In mammals, self-assembly of VPS41 is required for the biogenesis of the secretory pathway (Asensio et al., 2013) and mutations in this protein are related to neurological disorders and abnormal membrane trafficking (Sanderson et al., 2021) associated with lysosomal abnormalities (Steel et al., 2020). Likewise, deletions in VPS41

in pancreatic B cells cause defects in insulin secretion (Burns et al., 2021). In fungi, VPS41 also localizes to endosomes and vacuole membrane, and it is essential for plant infection and fungal development (Li et al., 2018). In *A. thaliana*, AtVPS41 controls pollen tube–stigma interaction and is found in pre-vacuolar compartments and in the tonoplast, where it is required for the late stage of the endocytic pathway (Hao et al., 2016). It is highly expressed in anthers and petals, followed by roots and cotyledons (Klepikova et al., 2016). This high expression in anthers fits with the inability to develop pollen tubes in some mutants, leading to male sterility (Hao et al., 2016). Additionally to its localization to the tonoplast, in root cells, AtVPS41 is also located to condensates that are essential for developmental regulation (Jiang et al., 2022). T-DNA insertion mutants in *Arabidopsis* seem to be lethal, revealing the fundamental role of VPS41, whereas *zip-2*, a single mutant in AtVPS41, shows no obvious phenotype (Niihama et al., 2009). Likewise, point mutations observed in melon CmVPS41 show no phenotype except impairing CMV phloem entry, suggesting that the main function of VPS41 has not been altered with these mutations (Giner et al., 2017; Pascual et al., 2019). VPS41 has also been related to Ebola and Marburg flaviviruses infection in humans (Carette et al., 2011).

Expression of CmVPS41PS transgene in the melon accession SC can complement CMV phloem entry, allowing a systemic infection (Giner et al., 2017). Although CmVPS41 is a general gatekeeper in many melon genotypes for viral phloem entry and determines the resistance against CMV-LS, its mechanism of action is yet to be characterized. Here we have investigated the localization pattern of CmVPS41 from both, susceptible and resistant melon genotypes, and the localization of CmVPS41 carrying only the mutations causing the resistance from some resistant accessions. We have also investigated their response to the presence of the viral MP and to the whole virus during the infection.

Results

CmVPS41 associates in vivo with CMV-FNY movement protein

Given that CMV-MP is the determinant of virulence that communicates with CmVPS41, we investigated if there was interaction between these two proteins. For yeast two hybrid (Y2H) experiments, yeast clones carrying either MP-FNY or MP-LS were tested against those carrying either CmVPS41PS or CmVPS41SC. After mating, the resulting colonies were as white as the negative control, while the positive control turned blue. This indicated that none of the MPs interacted with any of the CmVPS41s (Figure 1A). This experiment was repeated twice, getting the same result. To confirm this result in vivo, we performed bimolecular fluorescence complementation (BiFC) assay experiments using the constructs VPS41s-YN and MPs-YC, where the CmVPS41 from either PS or SC carried the N-terminal part of YFP, and the

MP from either CMV-FNY or CMV-LS carried the C-terminal part of YFP. Then, coagroinfiltration of the VPS41s-YN and MPs-YC BiFC constructs showed that MP-FNY was able to interact both with CmVPS41PS and CmVPS41SC in a pattern compatible with their localization at the plasmodesmata, whereas MP-LS was unable to interact with any CmVPS41. CmL-ascorbate oxidase was used as positive control for interaction with CMV-MP (Figure 1C). Negative controls were the same proteins alone (Supplemental Figure 1). To confirm that CMV-MPs localize at the PDs, we investigated the cellular localization of the CMV-MPs alone. Coagroinfiltration of a 35S:MP-FNY-GFP or 35S:MP-LS-GFP constructs with the PD marker plasmodesmata-located protein 1 (PDLP1; Amari et al., 2010) tagged with RFP, showed that, as expected, both MPs colocalize with PDLP1 at the PDs (Figure 1B). Therefore, the interaction between VPS41s and MP-FNY was taking place at or near the PDs. VPS41s-YN would also localize at the same localizations shown below (tonoplast, late endosome, plasma membrane) but it would only be visualized where CMV-MP was present. This experiment does not preclude the possibility that MP-FNY re-localizes at least part of CmVPS41 to PDs. Altogether, these experiments indicated that the only possible interaction was between the CmVPS41PS or CmVPS41SC with MP-FNY.

Localization pattern of CmVPS41 from resistant and susceptible melon genotypes is different

To analyze the subcellular localization of CmVPS41s, the genes from both, the susceptible melon genotype PS and the resistant SC, tagged with eGFP (Enhanced Green Fluorescence Protein), were expressed under a dexamethasone-inducible promoter in *Nicotiana benthamiana* epidermal cells. We observed that 20 h after dexamethasone application, both variants seem to localize to the cytoplasm and the nucleus. However, there were some differences in the expression pattern of both CmVPS41 variants. CmVPS41PS expression was very strong as spots in the plasma membrane or in the tonoplast and presented speckles in both, the nuclear membrane, and the nucleus. Also, there were several transvacuolar strands in most cells (Figures 1 and 2A). However, in the cells expressing the resistant allele, CmVPS41SC, there were no membrane spots, with few or no speckles, the expression inside the nucleus and cytoplasm was smooth, there were no transvacuolar strands and there were many tonoplast invaginations toward the vacuole (Figures 2A, 3, and 4). These localization patterns were clearly different from those shown when expressing eGFP alone (Supplemental Figure 2). Western blot analyses showed that both CmVPS41 proteins had been correctly expressed (Supplemental Figures 3 and 4, lanes 1 and 2). A quantification of the cells carrying these distinctive structures showed significant differences among the susceptible PS and the resistant SC variants (Figure 2B). More than 90% of cells expressing CmVPS41PS showed nuclear speckles, whereas in only 30% of cells expressing CmVPS41SC, some speckles could be found. The difference

in membrane or tonoplast spots was even more evident, since almost none of the CmVPS41SC-expressing cells showed them, whereas nearly all cells expressing CmVPS41PS presented them. The differences in transvacuolar strands were also significant, with most CmVPS41SC cells presenting one or none and most CmVPS41PS presenting a mean of four strands. Last, a mean of 75% of VPS41SC expressing cells showed tonoplast invaginations, whereas those structures were almost absent from CmVPS41PS-expressing cells. Thus, although both proteins localized in the cytoplasm, there were localization patterns clearly different in both CmVPS41s in some structures when expressed in *N. benthamiana* epithelial cells. From those structures, some of them (transvacuolar strands and nuclear and membrane/tonoplast spots) would be related with the susceptible variant, whereas the intravacuolar invaginations would be related with the resistant CmVPS41SC variant.

CmVPS41-induced differential structures colocalize with late endosomes

VPS41 is a protein involved in the transport of cargo proteins from late Golgi to the vacuole via either vesicles or endosomes. To identify the subcellular nature of the distinctive structures, a set of cell markers were used. As seen in Figure 3, CmVPS41 from both variants are identified in several organelles, including endoplasmic reticulum, plasma membrane, tonoplast, or late endosomes. However, the transvacuolar strands and the spots seen in CmVPS41PS expression and the invaginations from CmVPS41SC colocalize only with late endosome (Figure 3 and Supplemental Figure 2). Controls expressing the Ara6 late endosome marker alone does not show those typical structures (Supplemental Figures 5 and 6). Thus, the differential structures shown by expression of VPS41s are derived of late endosomes, and this suggests that the expression of both variants induces a different distribution of the endosomes throughout the cytoplasm, including crossing the vacuole from side to side and invaginations toward the vacuole.

CmVPS41-induced reorganization of late endosomes is not affected by the presence of CMV-MP

The determinant of virulence that relates to the *cmv1* gene (CmVPS41SC) is the MP (Guiu-Aragonés et al., 2015). As the MP from CMV-FNY enables the virus to overcome the resistance posed by *cmv1*, whereas the MP from CMV-LS does not, it might be possible that the localization pattern of CmVPS41SC could change in the presence of MP-FNY. As shown in Figure 4, coagroinfiltration experiments expressing both CmVPS41s and both CMV-MPs showed that the localization pattern of CmVPS41PS does not change significantly in the presence of either MP, showing no significant differences in nuclear speckles, membrane spots, and absence of intravacuolar invaginations. Only the presence of either MP seemed to decrease slightly the number of transvacuolar strands per cell (Figure 4B). Likewise, the localization of

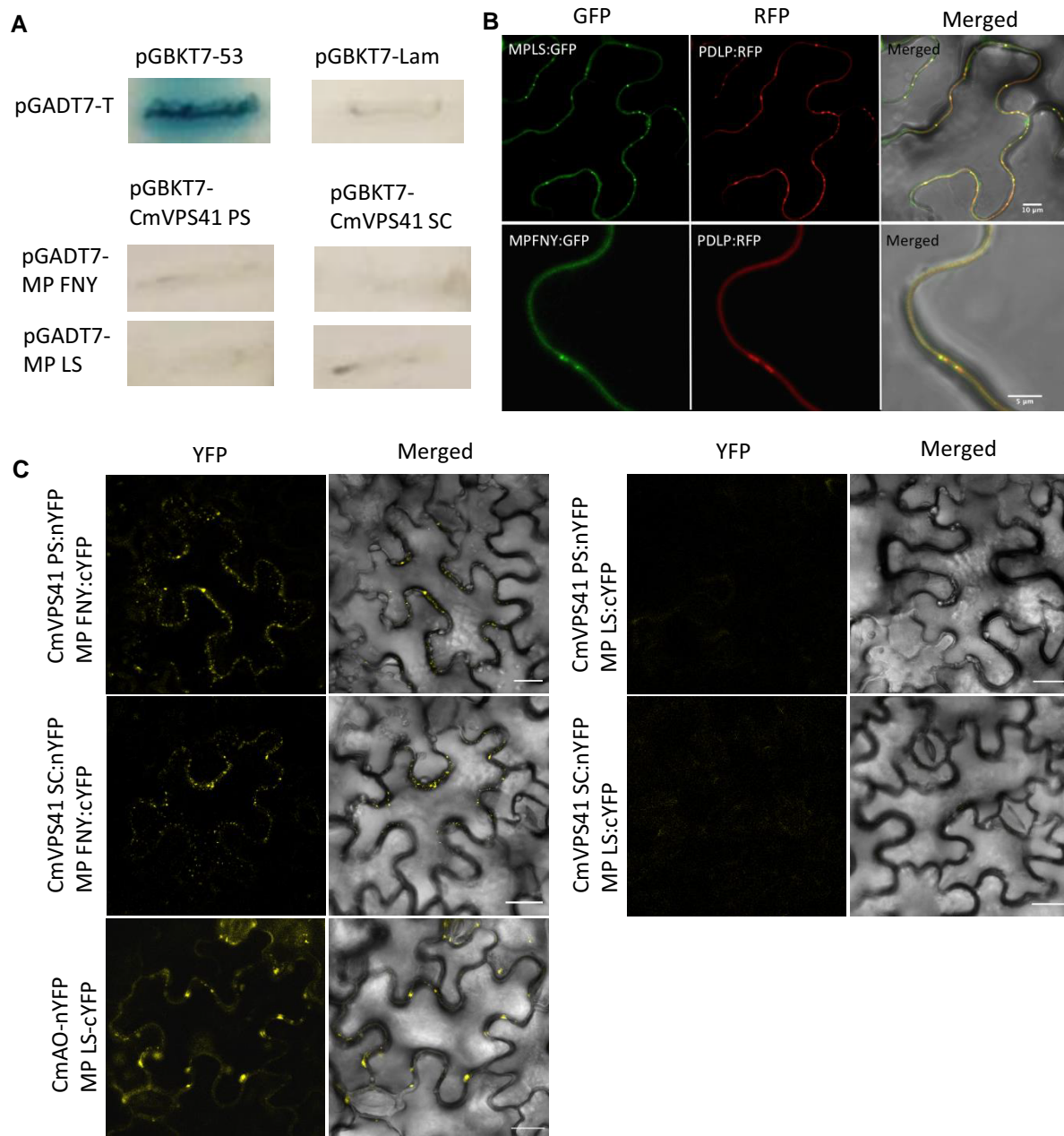


Figure 1 Interaction between CmVPS41s and CMV-MPs. A, Y2H between CmVPS41 and CMV-MPs in SD-Trp/-Leu/X-alpha-Gal/AbA/-His/-Ade agar plates. Each cell shows the results of Y2H interaction combination of prey in vector pGADT7 per bait in vector pGBKT7. Growth of a strong or light blue colony indicates interaction between prey and bait, while the absence of growth or white colonies indicates no interaction. Controls are pGADT7-T (prey) in combination with either bait pGBKT7-53 (positive interaction) or bait pGBKT7-Lam (no interaction). B, Colocalization of CMV-MPs (MP-FNY-GFP or MP-LS-GFP) with plasmodesmata marker (PDLP1-RFP). Colocalization of MPs and PDLP1 can be observed as yellow color. Scale bars are 10 μm for MP-LS and 5 μm for MP-FNY. C, In planta BiFC assay between CmVPS41s and CMV-MPs. CmAO-nYFP, *C. melo* L-ascorbate oxidase used as positive MP interacting control. "Merged": YFP and bright field channel together. BiFC scale bars correspond to 20 μm length.

CmVPS41SC did not change in the presence of either MP-LS or MP-FNY, showing no speckles, very few transvacuolar strands and most cells had tonoplast invaginations, like the pattern of the CmVPS41SC expressed alone (Figure 4B). These experiments were repeated three times with comparable results. Therefore, the coexpression of

CmVPS41SC with the MP-FNY does not induce any significant change in the localization of the CmVPS41SC that could resemble a susceptible pattern, more like that of CmVPS41PS. Additionally, Figure 4A shows that membrane spots do not colocalize with PDs, since those spots do not colocalize with MPs.

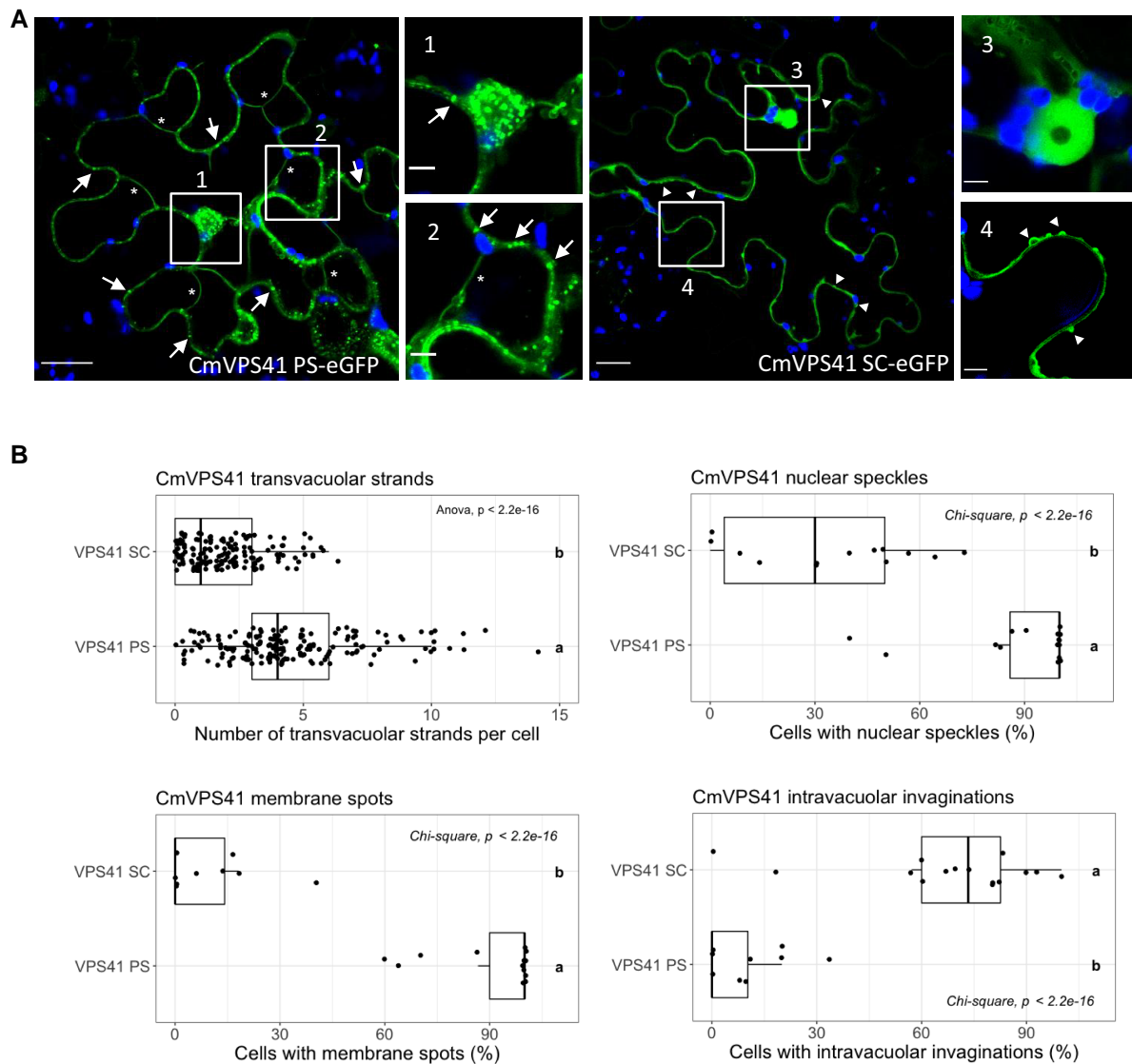


Figure 2 Localization patterns of CmVPS41. A, Localization of CmVPS41PS (CmVPS41 PS-eGFP) and CmVPS41SC (CmVPS41SC-eGFP). In blue, chloroplast autofluorescence. Image 3 shows the nucleus in a different Z-plane than in the whole image. Image scales from whole images correspond to 20 μm and amplified images scale is 5 μm . Arrows: membrane spots. Arrowheads: intravacuolar invaginations. *Transvacuolar strands. B, Boxplots of distinctive structures in CmVPS41PS and SC-expressing cells. The same letter corresponds to non-significant differences ($P > 0.05$) between CmVPS41PS and CmVPS41SC. The box ranges from the first quartile to the third quartile of the distribution and the range represents the IQR (interquartile range). A line across the box indicates the median. Top and bottom “whiskers” represent the highest or lowest values excluding outliers. For transvacuolar strands boxplot, each point represents the number of transvacuolar strands present in an individual cell. For the rest of boxplots, each point represents the percentage of cells that present the specific VPS41 structure.

CmVPS41 variants from resistant or susceptible melon genotypes have different localization patterns

The analysis of the CmVPS41 gene in 54 melon accessions had identified several previously unidentified resistant genotypes, among them, Freeman’s cucumber (FC) and Pat-81 (Pascual et al., 2019). CmVPS41 from SC differs from CmVPS41PS in three amino acid positions (P262A, L348R, and S620P). However, only the change L348R correlates with resistance to CMV (Giner et al., 2017; Pascual et al., 2019). Pat-81 and FC differ from PS in the same P262A,

S620P, and also in G85E instead of L348R (Pascual et al., 2019; Figure 5A). On the contrary, the accession Cabo Verde is a susceptible genotype that shared P262A and S620P amino acid polymorphisms with SC, FC, and Pat-81, but lacks any putative causal mutation (Figure 5A). Overexpression of CmVPS41 from both FC and Pat-81 genotypes, as well as from Cabo Verde, confirmed most of the above characteristics. CmVPS41 from Cabo Verde presented membrane spots and nuclear speckles, transvacuolar strands and very few intravacuolar invaginations, like PS does (Figure 5, B and C), whereas CmVPS41 from the accessions

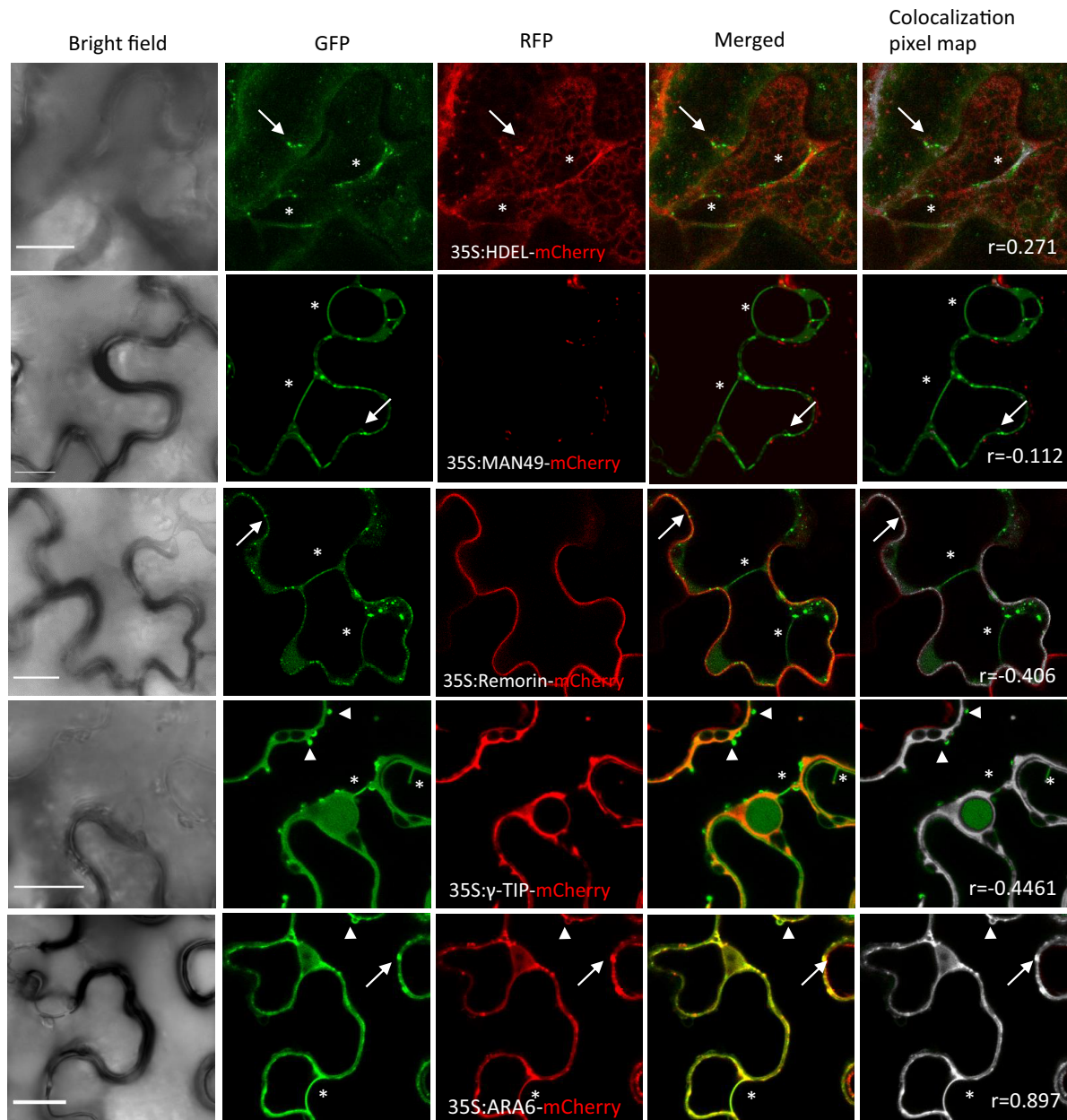


Figure 3 Colocalization of CmVPS41 with organelle markers. GFP channel: CmVPS41s specific structures. RFP channel: different organelle markers, endoplasmic reticulum (35S:HDEL-mCherry), Golgi apparatus (35S:MAN49-mCherry), plasma membrane (35S:Remorin-mCherry), tonoplast (35S:γ-TIP-mCherry), and late endosome (35S:ARA6-mCherry). Merged: colocalization is shown as a yellow color. Colocalization pixel map, shown in gray, while non-colocalized pixels keep the original color. Pearson correlation coefficient (r) of pixel matching colocalization was calculated with Fiji software analysis tool “Colocalization threshold.” Scale bars are 20 μm. Arrows indicate membrane spots. Arrowheads indicate intravacuolar invaginations. Asterisks indicate transvacuolar strands.

FC and Pat-81 showed smooth nuclei and cytoplasm and very few transvacuolar strands, like CmVPS41SC. However, unlike CmVPS41SC, they show very few intravacuolar invaginations (Figure 5, B and C). Thus, this suggests that the resistance to CMV would not be related to the presence of invaginations of the tonoplast. Western blot analyses showed that all proteins were expressed, although those from CV and FC in lower amount (Supplemental Figure 3). However, independently of the amount of protein expressed, PS and CV

susceptible accessions showed the same subcellular localization and the same is true for FC and Pat-81 resistant accessions (Figure 5, B and C).

The mutations causing resistance induce a decrease in the number of transvacuolar strands

To determine which of the structures were related to the causal mutations, and hence, to resistance, two constructs

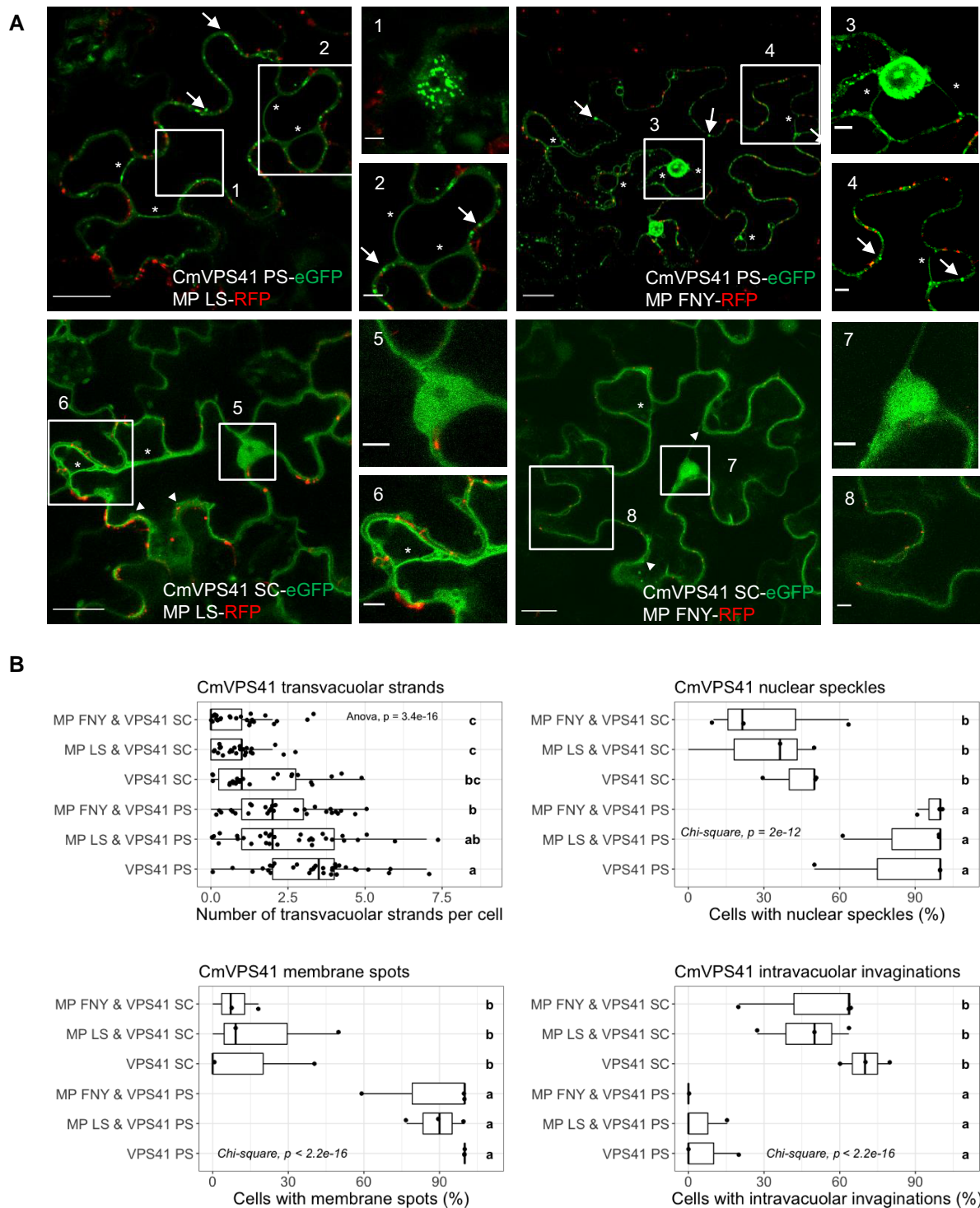


Figure 4 CMV-MPs effect on CmVPS41-induced structures. A, Colocalization of CmVPS41PS-eGFP or CmVPS41SC-eGFP with CMV-MP-FNY-RFP or CMV-MP-LS-RFP. Numbers indicate areas amplified on the right. Image 1 shows the nucleus in a different Z-plane than in the whole image. Scale bars are either 20 μm (whole image) or 5 μm (amplified image). Arrows indicate membrane spots. Arrowheads indicate intravacuolar invaginations. Asterisks indicate transvacuolar strands. B, Boxplots of CmVPS41-induced structures. The same letter corresponds to non-significant differences ($P > 0.05$) between CmVPS41PS and CmVPS41SC (coinfiltrated or not with CMV-MPs). Definition of the various elements of the boxplot is as in figure legend 2.

were built. Both kept the sequence of CmVPS41PS, but carried only the nucleotide change either at nucleotide 254, which produced the amino acid substitution G85E, or at

nucleotide 1,043, which expressed a VPS41 protein carrying the L348R change (Pascual et al., 2019). After infiltration into *N. benthamiana* plants, the construct carrying L348R

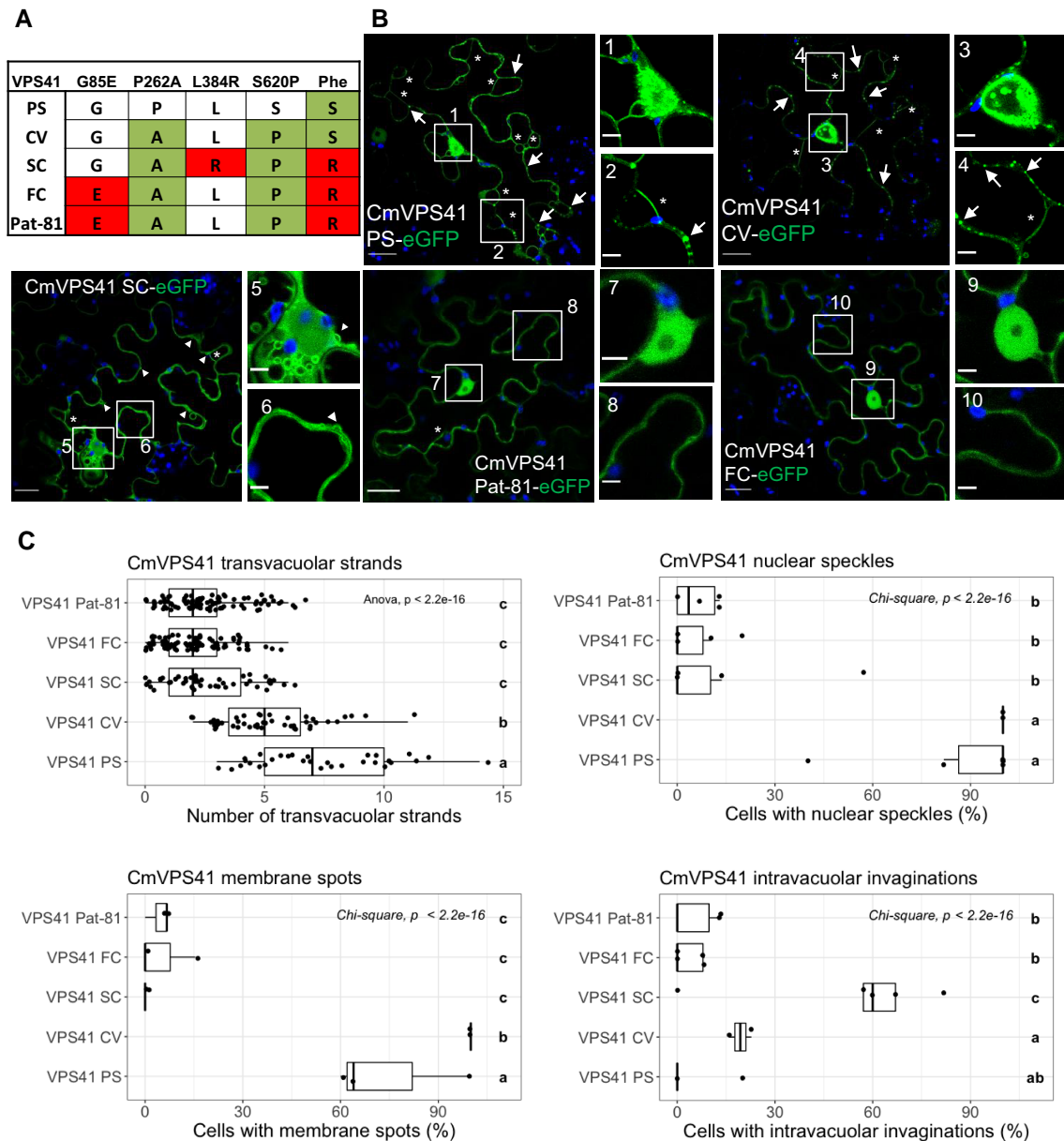


Figure 5 CmVPS41-induced structures in exotic melon genotypes. A, Amino acid changes of the CmVPS41 melon variants compared to CmVPS41PS. Phe, phenotype of the corresponding variant; S, susceptible to CMV-LS; R, resistant to CMV-LS. B, CmVPS41 distinctive structures in the melon genotypes CV (CmVPS41CV-eGFP), Pat-81 (CmVPS41Pat-81-eGFP), FC (CmVPS41FC-eGFP), PS (CmVPS41PS-eGFP), and SC (CmVPS41SC-eGFP). In blue, chloroplast autofluorescence. Scale bars are either 20 μm (whole images) or 5 μm (amplified images). Arrows indicate membrane spots. Arrowheads indicate intravacuolar invaginations. Asterisks indicate transvacuolar strands. C, Boxplots of CmVPS41 structures in CV, Pat-81, and FC compared with PS and SC. The same letter corresponds to non-significant differences ($P > 0.05$) between CmVPS41 genotypes. Definition of the various elements of the boxplot is as in figure legend 2.

lost the localization pattern of CmVPS41PS and showed many intravacuolar invaginations, fewer cells with membrane spots and nuclear speckles, and fewer transvacuolar strands. This is a typical CmVPS41SC localization (Figure 6, A and B). Moreover, the number of cells with intravacuolar invaginations was higher than when expressing CmVPS41SC and they appeared to be generated frequently

nearby the nuclear membrane. Therefore, the same mutation responsible for the resistance correlates with changes in the distribution of the late endosome to produce numerous intravacuolar invaginations and few transvacuolar strands. The overexpression of the CmVPS41 construct carrying the G85E causal mutation showed no cells with tonoplast invaginations and very few transvacuolar strands per cell

(Figure 6, A and B), which confirmed the observations made with Pat-81 and FC. The only difference with those accessions was the presence of some cells with membrane spots. Western blots demonstrated that all proteins were expressed, although the construct with the mutation L348R in lower amount (Supplemental Figure 4). However, irrespective of the amount of protein expressed, CmVPS41 L348R showed the same intracellular localization than the corresponding CmVPS41SC. Altogether, these results indicate that the lack of transvacuolar strands, rather than the presence of tonoplast invaginations, correlates with the mutations that cause resistance to CMV.

Some structures from both, resistant and susceptible CmVPS41s variants, re-localize during the viral infection

Although the MP is the virulence determinant of CMV against the gene *cmv1*, its coexpression under a strong promoter with CmVPS41 does not show an influence in the VPS41 localization pattern. However, during a real infection the MP can be expressed on due amount, from its own promoter, and time, since different viral proteins are expressed at different times in the infected cells, and this could lead to a change in the CmVPS41 localization. To analyze this, *N. benthamiana* plants were inoculated either with CMV-FNY or CMV-LS and, after the onset of symptom appearance, new, symptomatic leaves were tested for virus presence by reverse transcription-polymerase chain reaction (RT-PCR; Supplemental Figure 7) and then agroinfiltrated either with CmVPS41PS-GFP or CmVPS41SC-GFP. In these *N. benthamiana* infected cells, both CmVPS41PS and CmVPS41SC-infiltrated plants showed some differences in the localization pattern independently of the virus strain used. Nuclear speckles were present in many CmVPS41PS-expressing cells and much fewer in CmVPS41SC-expressing cells, like in non-infected infiltrated cells shown above (Figure 7). Conversely, the number of cells with membrane spots increased, and the number of tonoplast invaginations decreased in CmVPS41SC-expressing cells with respect to non-infected plants (Figure 7, A and B). Interestingly, transvacuolar strands remained very scarce for SC-expressing cells but in PS-infiltrated cells its number decreased significantly during the viral infection, suggesting that these strands could be transiently formed during a real infection and, once the infection is set, they could be no longer needed. Thus, two distinctive structures were differentially present in CMV-infected cells with respect to their non-infected counterparts: the number of cells with membrane spots increased in CMV-infected CmVPS41SC-expressing cells and the number of transvacuolar strands decreased in CmVPS41PS-expressing cells.

Discussion

VPS41, as a component of the HOPS complex, is a key regulator of cell trafficking. Here we have described the cellular localization of CmVPS41 both from the susceptible cultivar

PS and from the resistant exotic cultivar SC, showing that they have differences, mainly in membrane and nuclear speckles, transvacuolar strands and intravacuolar invaginations. Sometimes, these structures moved during the observation. Transvacuolar strands and intra vacuolar invaginations have already been described in soybean (*Glycine max*; Nebenführ et al., 1999) and in several cell types in *A. thaliana*, where these structures are moving and changing their morphology in a manner dependent on actin microfilaments. Furthermore, the movement of the transvacuolar strands was dependent on actin microfilaments (Uemura et al., 2002). Interestingly, CMV-MP has been involved in severing acting filaments to increase the size exclusion limit of plasmodesmata (Su et al., 2010). These transvacuolar structures have been related to the distribution of different solutes, mRNAs, and organelles, like Golgi vesicles in the cytoplasm up to the PDs. Moreover, the non-mobile RFP mRNA was targeted to PDs through the transvacuolar strands when coexpressed with tobacco mosaic virus MP, suggesting that these strands can be used by a viral MP to direct the virus toward the PDs (Luo et al., 2018). Thus, these structures could well be used also by CMV during the infection through its MP and, together with CmVPS41, for its intracellular movement toward the PDs. The localization of CmVPS41s carrying only the causal mutations for resistance L348R (Giner et al., 2017) and G85E (Pascual et al., 2019), indicated that the resistance was mostly related to the absence of transvacuolar strands, rather than with the presence of intravacuolar invaginations, which supports the idea that those strands could be involved in CMV intracellular trafficking. A more exhaustive analysis with three-dimensional visualization of confocal stack images shows the structure of these transvacuolar strands, appearing as ropes arranged in a fence-like manner (Figure 8). The special structures colocalize with late endosomes, which is one of the ways the CmVPS41, as part of the HOPS complex, carries cargo proteins to the vacuole. The other way, the AP-3 pathway, skips the endosome pathway and needs VPS41 to drive vesicles directly to the vacuole (Rehling et al., 1999). Thus, the late endosomal localization of the differential structures observed in our experiments suggests that CMV uses CmVPS41 in the endosomal pathway and is independent of the vesicle transport of the AP-3 pathway. Furthermore, as the coexpression with the viral MP does not have an effect in the differential structures present with CmVPS41SC, probably MP alone is not redirecting endosomal trafficking of CmVPS41 and the way in which these two proteins cooperate remains to be seen.

Despite the MP being the determinant of virulence that communicates with CmVPS41 during infection, overexpression of CmVPS41s with CMV-MPs does not change significantly the CmVPS41SC localization. This would suggest that either the differential structures are not really related to resistance to CMV or that the MP does not participate at this step of the infection. Alternatively, in the context of a viral infection, it may need the participation of other viral

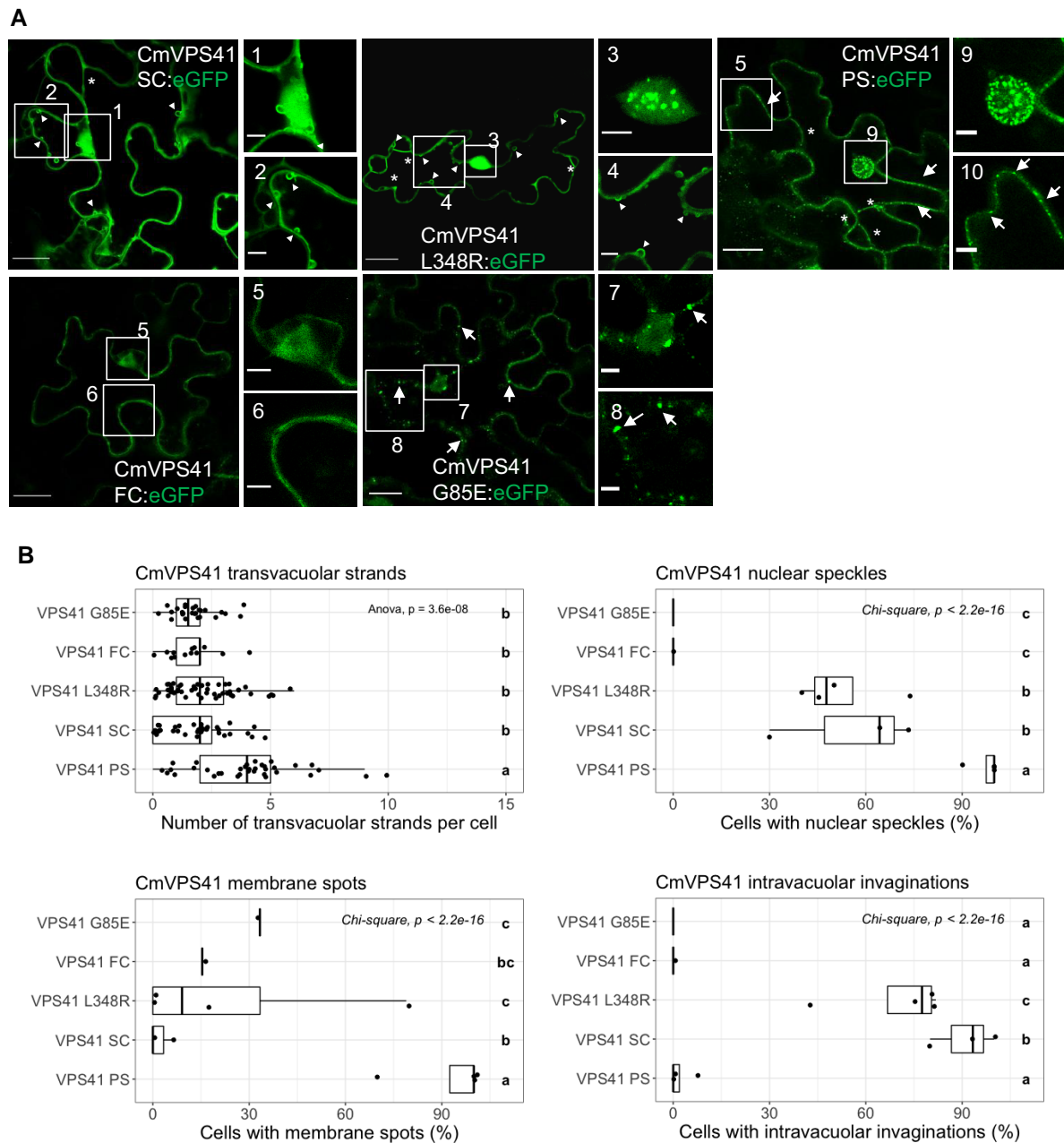


Figure 6 Effect of causal mutations on CmVPS41 structures. A, Localization of CmVPS41 carrying different causal mutations. CmVPS41 G85E-eGFP and CmVPS41 L348R-eGFP carry the causal mutations G85E and L348R, respectively. CmVPS41PS-eGFP, CmVPS41SC-eGFP, and CmVPS41FC-eGFP correspond to PS, SC, and FC genotypes, respectively. Bar scales are either 20 μm (whole images) or 5 μm (amplified images). Arrows indicate membrane spots. Arrowheads indicate intravacuolar invaginations. Asterisks indicate transvacuolar strands. B, Boxplots of CmVPS41 structures. The same letter corresponds to non-significant differences ($P > 0.05$) between different treatments. Definition of the various elements of the boxplot is as in figure legend 2.

proteins to fully re-localize those differential structures. In fact, overexpression of CmVPS41s in systemically infected *N. benthamiana* leaves showed a similar localization pattern with both proteins, presenting many cells with membrane spots, very few transvacuolar strands per cell and very few cells with intravacuolar invaginations. Only nuclear speckles were behaving as in the absence of infection, abundant in PS and scarce in SC. Membrane spots do not colocalize with

PDs, since they do not colocalize with MPs. Besides, membrane spots are not related to cell-to-cell viral movement, since in the resistant accessions CMV can move cell-to-cell in the inoculated leaf until reaching the BS cells (Guiu-Aragonés et al., 2016). In the context of viral infection, not only the MP is present, but all viral proteins, whose expression should be tightly regulated. For example, some MPs, accumulate transiently in the first stages of the cell

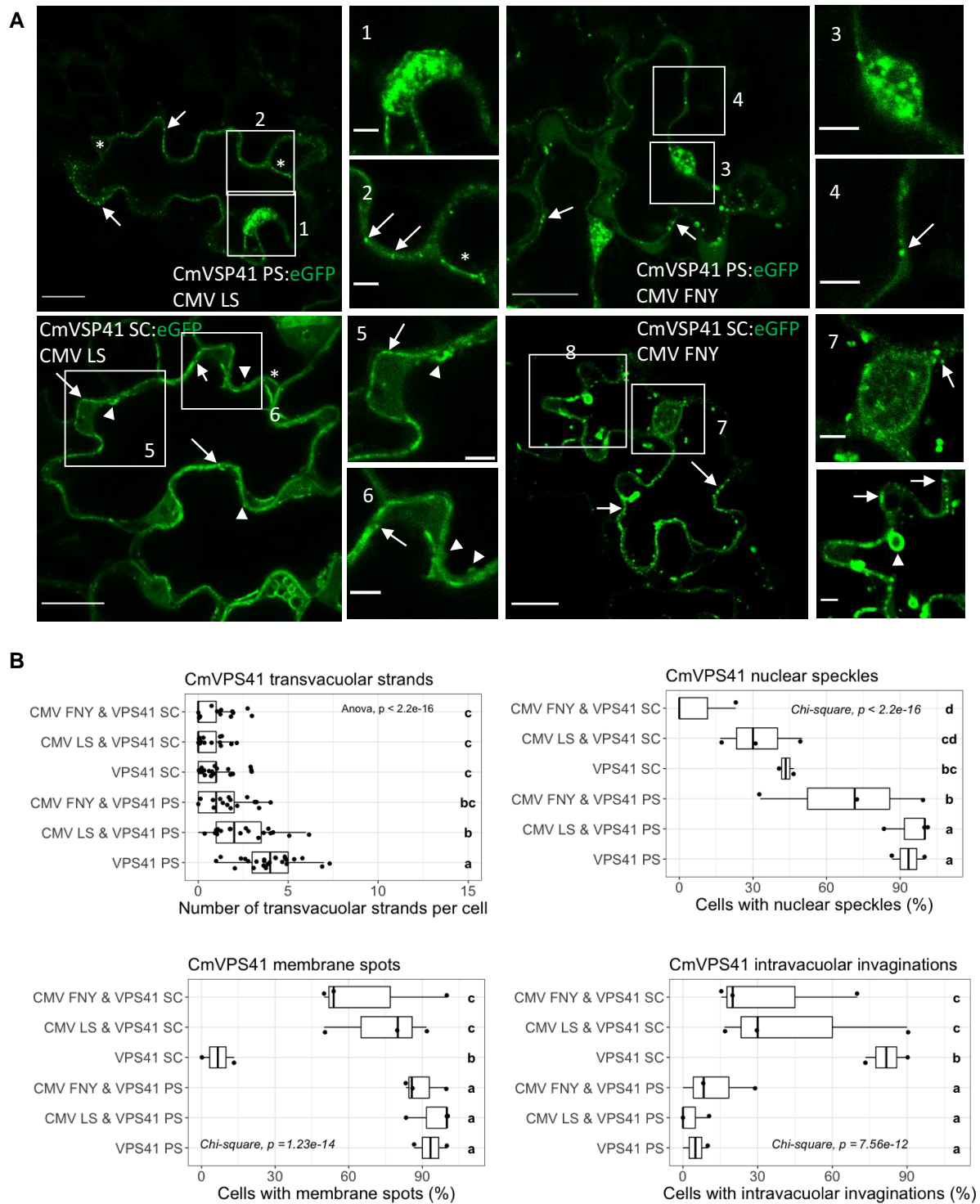


Figure 7 Effect of CMV infection on CmVSP41 structures. A, Localization of CmVSP41PS-eGFP or CmVSP41SC-eGFP in either CMV-LS or CMV-FNY infected leaves. Bar scales are either 20 μm (whole images) or 5 μm (amplified images). Arrows indicate membrane spots. Arrowheads indicate intravacuolar invaginations. Asterisks indicate transvacuolar strands. B, Boxplots of CmVSP41 structures. The same letter corresponds to non-significant differences ($P > 0.05$) between different treatments. Definition of the various elements of the boxplot is as in figure legend 2.

infection (Maule and Palukaitis, 1991). The fact that the transvacuolar strands are dynamic (Uemura et al., 2002), suggests that, when the infection is fully established, these structures may disappear, since they may not be further needed

for moving the virus toward the PDs. One possible mechanism for the dynamism of these structures during viral infection may be the timely degradation by the Ubiquitination Proteasome System (UPS). Many viral proteins are degraded

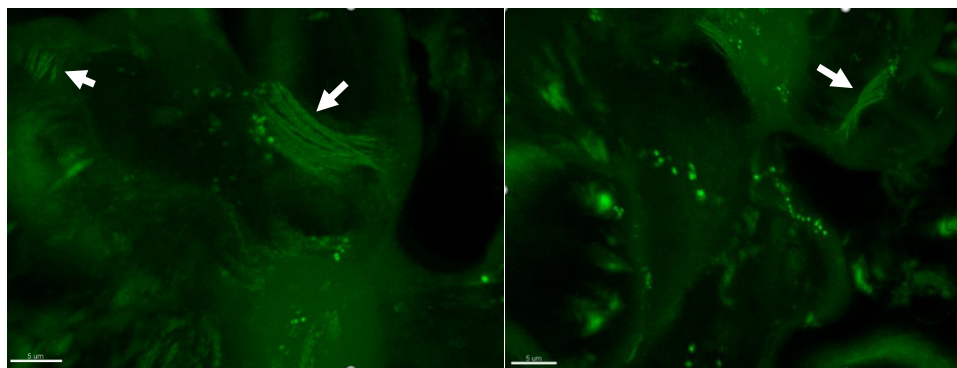


Figure 8 Three-dimensional reconstruction from Z-stack of CmVPS41PS-derived transvacuolar strands. Arrows indicate transvacuolar strands. Scale bars are 5 µm.

in vivo by the UPS, among them, TMV MP as well as those MPs from turnip yellow mosaic virus, potato leafroll virus, and TGBp3 from potato virus X are known proteasome degraded viral MPs (Reichel and Beachy, 2000; Drugeon and Jupin, 2002; Vogel et al., 2007; Ju et al., 2008). Thus, UPS degradation of viral proteins, and particularly MPs, seems to be a quite extended regulation system in viral infections (for a review, see in Alcaide-Loridan and Jupin, 2012). Thus, the interplay of all viral proteins and their timely regulation during infection could render a CmVPS41 localization pattern quite different in different times of the infection and different than when overexpressed with MP. Further work is needed to unveil the role of CmVPS41-produced transvacuolar strands during CMV infection and the link with factors that regulate VPS41 function, such as the levels of phosphatidylinositol or the role of Rab GTPases (Brillada et al., 2018).

Materials and methods

Plant material, viral strains, and yeast strains

Melon (*C. melo* L.) genotypes, Piel de Sapo (PS), SC, FC, Pat-81, and Cabo Verde (CV), with different susceptibilities to CMV were used to clone their corresponding CmVPS41 genes (Supplemental Table 1). The list of CmVPS41 included two chimerical constructs with CmVPS41 genotype from PS carrying the identified causal mutations: (1) causal mutation present in cultivar SC (L348R; Giner et al., 2017) and (2) causal mutation found in cultivars FC and Pat 81 (G85E; Pascual et al., 2019). *Cucumis melo* L. seeds were pregerminated by soaking them in water overnight, and then maintained for 2–6 days in neutral day at 28°C. Seedlings were grown in growth chambers SANYO MLR-350H in long-day conditions consisting of 22°C for 16 h with 5,000 lux of light and 18°C for 8 h in the dark. For agroinfiltration, *N. benthamiana* plants were grown in the greenhouse in long-day conditions consisting of 24–28°C with 5,000 lux of light for 16 h and 22–24°C 8 h in the dark.

CMV strains CMV-LS and CMV-FNY were used for CMV infection assay. *Saccharomyces cerevisiae* strains Y2HGold

and Y187 were used for Y2H assay (Takara Bio, Mountain View, CA, USA).

Plasmid construction

For colocalization experiments with CmVPS41s, total RNA extractions from the different melon accessions were performed using TriReagent (Sigma-Aldrich, St Louis, MO, USA) following the manufacturer's protocol. 200 ng of total RNA were used to synthesize cDNA using oligo (dT)_{12–18} primer (Invitrogen by Thermo Fisher Scientific, Vilnius, Lithuania) and PrimeScript (Takara Bio, Dalian, China), according to manufacturer's instructions. For cloning the complete CmVPS41 genes, cDNA was PCR amplified using the PrimeSTAR[®] GXL DNA Polymerase (Takara Bio, Dalian, China) and the primers annealing at the ends of the gene and carrying the attB sequences (Supplemental Table 1) and cloned into the pBSDONR P1–P4 (Gu and Innes, 2011) by Gateway BP reaction (MultiSite Gateway[®] Pro from Invitrogen by Thermo Fisher Scientific, Vilnius, Lithuania). For CmVPS41 clones carrying the causal mutations, CmVPS41 G85E and L348R constructs were generated from CmVPS41 pBSDONR P1–P4 VPS41PS and VPS41SC (for L348R) or VPS41PS and VPS41FC (for G85E) constructs using a combination of specific primers (Supplemental Table 1) to transfer the fragments containing the causal mutations to the VPS41PS background using Gibson Assembly technology (GeneArt[®] Seamless PLUS Cloning and Assembly Kit; Invitrogen Corporations, Carlsbad, CA, USA). eGFP (Cormack et al., 1996) and RFP (Campbell et al., 2002) were cloned into pBSDONR P4r-P2 for C-terminal fusion using specific primers. The P1–P4 clones were mixed with the corresponding P4r-P2 and the dexamethasone-inducible destination vector pBAV154 (Vinatzer et al., 2006) in a three-way Gateway LR reaction (MultiSite Gateway[®] Pro from Invitrogen by Thermo Fisher Scientific, Vilnius, Lithuania).

For MP localization experiments, the whole MP gene of both strains was PCR amplified using primers that generate *Bam*HI and *Xho*I at 5' and 3' end of gene, respectively. PCR products were cloned into GATEWAY[®] pENTR[™] 3C (Invitrogen Corporations) at *Bam*HI-*Xho*I sites. To express

C-terminally tagged fluorescent protein fusion of MP:GFP, both pENTR-MP-LS and pENTR-MP-FNY were recombined with destination vector pH7WGF2 (Karimi et al., 2002), using LR clonase mix (Invitrogen Corporations) according to the manufacturer's instructions. pDLP1:GFP clone was kindly provided by Prof Andy Maule (John Innes Centre) For BiFC assay, MPs and CmVPS41s coding sequences were PCR amplified using specific primers (Supplemental Table 1) and cloned into pDONR P1–P4 as described above, and introduced into the expression vector pBAV154 as a C-terminal fusion with either partial N-terminal YFP (YN) (for CmVPS41s) or partial C-terminal YFP (YC) (for CMV-MPs; Supplemental Table 2) using Gateway technology, as previously described.

For Y2H experiments, coding sequences of CMV-MPs and CmVPS41s were PCR amplified using specific primers (Supplemental Table 1) and cloned into plasmid pENTR/D-TOPO (Thermo Scientific by Thermo Fisher Scientific, Vilnius, Lithuania). Both MP genes were cloned into the pGBKT7 vector at the *Bam*HI and *Eco*RI sites using T4 DNA ligase (Thermo Scientific by Thermo Fisher Scientific, Vilnius, Lithuania) following manufacturer's instructions. CmVPS41s were cloned into pGADT7 vector at the *Sal*I and *Eco*RI sites using T4 DNA ligase (Thermo Scientific by Thermo Fisher Scientific, Vilnius, Lithuania).

For colocalization of CmVPS41 with organelle markers, *Arabidopsis* (*A. thaliana*) genes were used (Supplemental Table 2). Markers for Endoplasmic reticulum (35S:HDEL-mCherry), Golgi apparatus (35S:MAN49-mCherry), Tonoplast (35S:γ-TIP-mCherry), and late endosome (ARA6-mCherry) were from (Serrano et al., 2016). Plasma membrane marker (35S:Remorin-mCherry) was nicely provided by Dr Núria Sanchez Coll (CSIC, CRAG, Barcelona, Spain; Marín et al., 2012).

All constructs were verified by sequencing with Sanger method using an ABI 3730 DNA Analyzer (Applied Biosystems) for capillary electrophoresis and fluorescent dye terminator detection. Correct insertion and orientation of all constructs were verified with Sequencher® version 5.0 sequence analysis software (Gene Codes Corporation, Ann Arbor, MI, USA; <http://www.genecodes.com>). Correct plasmids were transformed into *Agrobacterium tumefaciens* GV3101.

Transient expression in *Nicotiana benthamiana*

Agrobacterium tumefaciens cultures carrying the corresponding plasmid were incubated at 28°C with their corresponding antibiotics for 24–48 h and bacterial pellet was collected by centrifugation and resuspended in induction buffer (10 mM MgCl₂ and 0.15 mM acetosyringone) to 0.4 final OD₆₀₀, except for the 35S:Remorin 1.3-mCherry experiments, where 0.2 final OD₆₀₀ was used. Bacterial culture was induced for 2 h in the dark. For agroinfiltration of more than one plasmid, suspensions were mixed in equal ratio and were infiltrated using a needleless syringe into the abaxial side of expanding third or fourth leaves of 2- to 3-week-old *N. benthamiana*

plants. For dexamethasone-inducible pBAV154-derived constructs, 24 h post infiltration, expression was induced applying 50 μM dexamethasone solution with a brush in the adaxial part of the infiltrated leaf (Sigma-Aldrich). Expression of fluorescence was observed at 20 h after dexamethasone induction in pBAV154-derived vectors and 48 h after agroinfiltration in vectors with 35S promoter.

Yeast two hybrid assays

Constructs for Y2H were freshly transformed into *S. cerevisiae* strains before every one-to-one Y2H assay. pGBKT7-MPs, positive control (pGBKT7-53), and negative control bait plasmids (pGBKT7-Lam) were transformed into yeast strain Y2HGold (Takara Bio, Mountain View, CA, USA) while pGADT7-CmVPS41s and pGADT7-T control prey plasmids were transformed into yeast strain Y187 following the Yeastmaker Yeast Transformation System 2 instructions (Clontech by Takara Bio, Mountain View, CA, USA). The transformed cells were grown either in SD-Trp agar plates for Y2HGold or in SD-Leu agar plates for Y187 at 30°C for 3–5 days. Matings between the Y2HGold and Y187 strains carrying the appropriate constructs were performed in 0.5 mL of 2X YPDA in the presence of the corresponding antibiotics following manufacturer's instructions (Clontech's Matchmaker Gold Yeast Two-Hybrid System, Clontech by Takara Bio, Mountain View, CA, USA). Yeast cells were cultured at 30°C for 24 h and plated in SD-Trp/-Leu/X-alpha-Gal agar plates. After 3–5 days, blue or white colonies appeared and were transferred in a more restrictive media (SD-Trp/-Leu/X-alpha-Gal/Aureobasidin A agar plates). After 5–7 days blue colonies (or in its defect white colonies) were selected and plated in the most restrictive media (SD-Ade/-His/-Trp/-Leu/X-α-Gal/AbA). True interaction was assumed when strong blue colonies were able to grow in the more restrictive media.

CMV inoculations

Viral inocula were freshly prepared from infected zucchini squash Chapin F1 (*Cucurbita pepo* L.; Semillas Fitó SA, Barcelona, Spain). Sap was rub-inoculated in first and second true leaves of 2-week-old *N. benthamiana* plants.

Virus detection

First true leaf of two *N. benthamiana* plants was inoculated with either CMV-LS or CMV-FNY. After detection of the symptoms, one leaf of each plant was collected at 2- and 3-weeks post inoculation. RNA was isolated, and the presence of the virus in the leaves was tested by RT-PCR as described (Guiu-Aragonés et al., 2015). CMV-LS, specific primer LS1-1400R, LS2-1400R, LS3-1400R, PCR1-1400R, PCR2-1400R, and PCR2-1400R were used for Reverse transcription reaction. The same primers, together with LS1-900F, LS2-900F, LS3-900F, FNY1-900F, FNY2-900F, and FNY3-900F, were used to amplify a 500-bp fragment of each RNA from the viral genome (Supplemental Table 1).

Confocal laser scanning microscopy

For BiFC and colocalization experiments of plasma membrane or endoplasmic reticulum with CmVPS41 proteins, images were collected on a Leica TCS-SP5 II confocal microscope (Leica Microsystems, Exton, PA USA) using a 63x water immersion objective NA 1.2, zoom 1.6. In BiFC images, YFP was excited with the blue argon ion laser (514 nm), and emitted light was collected between 530 and 630 nm using a HyD detector. For BiFC experiments, gain was always kept at 150. For colocalization, eGFP was excited with the blue argon ion laser (488 nm), and emitted light was collected between 495 and 535 nm. mCherry and RFP were excited with an orange HeNe laser (594 nm), and emitted light was collected between 570 and 660 nm. Chloroplasts were excited with the blue argon laser (488 nm), and emitted light was collected at 650–750 nm. eGFP and chloroplast signals were collected separately from the mCherry or RFP signals and later superimposed. We adjusted each image to avoid saturated pixels. All images were processed using Fiji imaging software (version 1.52i). Fiji colocalization tool “Colocalization Threshold” was used to calculate the Pearson coefficient of colocalization and to create a colocalized Pixel Map for each combination of CmVPS41 plus organelle marker. To observe CmVPS41 transvacuolar strands IMARIS software (Bitplane AG, Zurich, Switzerland) was used to perform 3D reconstructions of the Z-stacks of confocal images and capture snapshots.

In all other agroinfiltration experiments, images were collected on Olympus FV1000 confocal laser scanning microscope (Olympus, Tokyo, Japan). During scanning, we used a quadruple-dichroic mirror (DM 488/559). For visualization of eGFP, RFP, mCherry, and chloroplasts, the same emission and collection windows than for the Leica Microscope were used. The images with colocalization were studied by sequential excitation with each laser separately to avoid crossed fluorescence in the red channel. Images were processed using Olympus FV1000 software (version 04.02). Fiji (1.52i) was used to set the scale bar and calculate the Pearson coefficient for colocalization experiments with CmVPS41 and organelle markers.

Counting structures

The data come from at least three different transient assays and for each treatment, three biological replicates were used. In each experiment three plants were agroinfiltrated with the same construct in the same conditions and 15–20 cells were counted in one leaf. To count the differential structures, the expression of the constructs in all biological replicates was checked to check that the constructs were evenly expressed in all biological replicates. In all agroinfiltrated leaves (third to fourth), $\times 10$ objective was used to find areas where cells were expressing the constructs and conserved a normal cell structure. Then, a $\times 60$ objective was used to count the differential structures, all in the same cell. In each cell, all transvacuolar strands were counted by moving from the top to the bottom of the cell volume (Z-plane). The nuclei, membrane spots

and intravacuolar invaginations were annotated as presence/absence and expressed as percentage of cells showing that particular structure.

Data analysis

One-way analysis of variance ($P < 0.05$) was performed between CmVPS41 transvacuolar strands and each treatment. Upon significance, Tukey's test for post-hoc analysis was performed to group treatments with non-significant differences (same letter in boxplots). Chi-squared analysis ($P < 0.05$) was performed between each treatment and the rest of CmVPS41 structures using the raw data, counting presence/absence of the specific structure. Upon significance, Bonferroni's test for post-hoc analysis was performed to group treatments with non-significant differences (same letter in boxplots). For graphical representation, all boxplots were generated with R package “ggpubr.” For CmVPS41 transvacuolar strands boxplots, the number of transvacuolar strands per cell was plotted. For the rest of structures, the percentage of cells showing the corresponding CmVPS41 structure (nuclear speckles, membrane spots, or intravacuolar invaginations) was plotted. All boxplots contain the P -value from their corresponding analysis, as well as the results from the according post-hoc test.

Western blot

For determining the right expression of CmVPS41s proteins, 30 mg of frozen leaf powder per agroinfiltration were used. Protein extraction was carried out directly in 100 μ L sodium dodecyl sulfate (SDS) sample buffer (2% [w/v] SDS, 62.5 mM Tris-HCl [pH 6.8], 10% [v/v] glycerol, and 0.007% [w/v] bromophenol blue) including 50 mM DTT (Dithiothreitol) and protease inhibitor (Roche) and then boiled (95°C) for 5 min. 30 μ L were loaded and resolved on 6% (w/v) SDS gels and transferred onto nitrocellulose membranes with Mini-PROTEAN III and Mini Trans-Blot cells (Bio-Rad, Hercules, CA, USA), respectively, following conventional protocols. Uniform protein loading and transfer efficiency were verified by Ponceau staining of membranes. Primary antibody was anti-green fluorescent protein (mouse anti-GFP, Abcam, Cambridge, UK; Ab291-50, 1:1,000). The secondary antibody was anti-mouse IgG horseradish peroxidase conjugate (Sigma). Immunoreactive proteins were detected by chemiluminescence using the SuperSignal West Femto kit (Pierce, Thermo Fisher Scientific, Waltham, MA, USA).

Accession numbers

Sequence data from CmVPS41 from this article can be found in the Melonomics.net data library under accession number MELO3C004827.

Supplemental data

The following materials are available in the online version of this article.

Supplemental Figure S1. In planta BiFC negative controls for CmVPS41s and CMV-MPs interaction.

Supplemental Figure S2. Localization of eGFP fluorescence.

Supplemental Figure S3. Western blot analysis of CmVPS41 exotic melon accessions in *N. benthamiana* leaf extracts.

Supplemental Figure S4. Western blot analysis of VPS41 mutations causing resistance in *N. benthamiana* leaf extracts.

Supplemental Figure S5. Colocalization of CmVPS41 with late endosome.

Supplemental Figure S6. Localization pattern of late endosome maker (35S:ARA6-mCherry).

Supplemental Figure S7. Reverse transcription-PCR (RT-PCR) of young leaves from two CMV-infected individual *N. benthamiana* plants per virus strain.

Supplemental Table S1. Primers used in this study.

Supplemental Table S2. Constructs used in this study.

Acknowledgment

The authors thank Fuensanta Garcia for her technical support.

Funding

This work was supported by the grants AGL2015-64625-C2-1-R and RTI2018-097665-B-C2, from the Spanish Ministry of Economy and Competitiveness (cofunded by FEDER funds) and by the CERCA Programme/Generalitat de Catalunya. The authors acknowledge financial support from the Spanish Ministry of Science and Innovation-State Research Agency (AEI), through the “Severo Ochoa Programme for Centres of Excellence in R&D” 2016-2019 (SEV-2015-0533) and CEX2019-000902-S.

Conflict of interest statement. None declared.

References

- Alcaide-Loridan C, Jupin I (2012) Ubiquitin and plant viruses, let's play together! *Plant Physiol* **160**(1): 72–82
- Amari K, Boutant E, Hofmann C, Schmitt-Keichinger C, Fernandez-Calvino L, Didier P, Lerich A, Mutterer J, Thomas CL, Heinlein M, et al. (2010) A family of plasmodesmal proteins with receptor-like properties for plant viral movement proteins. *PLoS Pathog* **6**(9): e1001119
- Asensio CS, Sirkis DW, Maas JW, Egami K, To T-L, Brodsky FM, Shu X, Cheng Y, Edwards RH (2013) Self-assembly of VPS41 promotes sorting required for biogenesis of the regulated secretory pathway. *Dev Cell* **27**(4): 425–437
- Balderhaar HJK, Ungermann C (2013) CORVET and HOPS tethering complexes—coordinators of endosome and lysosome fusion. *J Cell Sci* **126**(6): 1307–1316
- Brillada C, Zheng J, Krüger F, Rovira-Díaz E, Askani JC, Schumacher K, Rojas-Pierce M (2018) Phosphoinositides control the localization of HOPS subunit VPS41, which together with VPS33 mediates vacuole fusion in plants. *Proc Natl Acad Sci U S A* **115**(35): E8305–e8314
- Burns CH, Yau B, Rodriguez A, Triplett J, Maslar D, An YS, van der Welle REN, Kossina RG, Fisher MR, Strout GW, et al. (2021) Pancreatic β -cell-specific deletion of VPS41 causes diabetes due to defects in insulin secretion. *Diabetes* **70**: 436–448
- Campbell RE, Tour O, Palmer AE, Steinbach PA, Baird GS, Zacharias DA, Tsien RY (2002) A monomeric red fluorescent protein. *Proc Natl Acad Sci U S A* **99**(12): 7877–7882
- Carette JE, Raaben M, Wong AC, Herbert AS, Obernosterer G, Mulharker N, Kuehne AI, Kranzusch PJ, Griffin AM, Ruthel G, et al. (2011) Ebola virus entry requires the cholesterol transporter Niemann-Pick C1. *Nature* **477**(7364): 340–343
- Cormack BP, Valdivia RH, Falkow S (1996) FACS-optimized mutants of the green fluorescent protein (GFP). *Gene* **173**(1): 33–38
- Drugeon G, Jupin I (2002) Stability in vitro of the 69K movement protein of Turnip yellow mosaic virus is regulated by the ubiquitin-mediated proteasome pathway. *J Gen Virol* **83**(12): 3187–3197
- Edwardson JR, Christie RG (1991) Cucumoviruses. In Edwardson JR, Christie RG, eds. *CRC Handbook of Viruses Infecting Legumes*. CRC Press, Boca Raton, FL, pp 293–319
- Essafi A, Diaz-Pendon JA, Moriones E, Monforte AJ, Garcia-Mas J, Martín-Hernández AM (2009) Dissection of the oligogenic resistance to *Cucumber mosaic virus* in the melon accession PI 161375. *Theor Appl Genet* **118**(2): 275–284
- Giner A, Pascual L, Bourgeois M, Gyetvai G, Rios P, Picó B, Troadec C, Bendahmane A, Garcia-Mas J, Martín-Hernández AM (2017) A mutation in the melon vacuolar protein sorting 41 prevents systemic infection of *Cucumber mosaic virus*. *Sci Rep* **7**(1): 10471
- Gu Y, Innes RW (2011) The KEEP ON GOING protein of *Arabidopsis* recruits the ENHANCED DISEASE RESISTANCE1 protein to trans-Golgi network/early endosome vesicles. *Plant Physiol* **155**(4): 1827–1838
- Guiu-Aragonés C, Díaz-Pendón JA, Martín-Hernández AM (2015) Four sequence positions of the movement protein of *Cucumber mosaic virus* determine the virulence against *cmv1*-mediated resistance in melon. *Mol Plant Pathol* **16**(7): 675–684
- Guiu-Aragonés C, Monforte AJ, Saladié M, Corrêa RX, Garcia-Mas J, Martín-Hernández AM (2014) The complex resistance to *Cucumber mosaic cucumovirus* (CMV) in the melon accession PI 161375 is governed by one gene and at least two quantitative trait loci. *Mol Breed* **34**(2): 351–362
- Guiu-Aragonés C, Sánchez-Pina MA, Díaz-Pendón J, Peña EJ, Heinlein M, Martín-Hernández AM (2016) *Cmv1* is a gate for *Cucumber mosaic virus* transport from bundle sheath cells to phloem in melon. *Mol Plant Pathol* **17**(6): 973–984
- Hao L, Liu J, Zhong S, Gu H, Qu LJ (2016) AtVPS41-mediated endocytic pathway is essential for pollen tube-stigma interaction in *Arabidopsis*. *Proc Natl Acad Sci U S A* **113**(22): 6307–6312
- Hashimoto M, Neriya Y, Yamaji Y, Namba S (2016) Recessive resistance to plant viruses: potential resistance genes beyond translation initiation factors. *Front Microbiol* **7**: 1695
- Hipper C, Brault V, Ziegler-Graff V, Revers F (2013) Viral and cellular factors involved in phloem transport of plant viruses. *Front Plant Sci* **4**: 154
- Jiang D, He Y, Zhou X, Cao Z, Pang L, Zhong S, Jiang L, Li R (2022) *Arabidopsis* HOPS subunit VPS41 carries out plant-specific roles in vacuolar transport and vegetative growth. *Plant Physiol* **189**(3): 1416–1434
- Ju HJ, Ye CM, Verchot-Lubicz J (2008) Mutational analysis of PVX TGBp3 links subcellular accumulation and protein turnover. *Virology* **375**(1): 103–117
- Karchi Z, Cohen S, Govers A (1975) Inheritance of resistance to *cucumber mosaic virus* in melons. *Phytopathology* **65**(4): 479–481
- Karimi M, Inzé D, Depicker A (2002) GATEWAY Vectors for *Agrobacterium*-mediated plant transformation. *Trends Plant Sci* **7**(5): 193–195
- Klepikova AV, Kasianov AS, Gerasimov ES, Logacheva MD, Penin AA (2016) A high resolution map of the *Arabidopsis thaliana* developmental transcriptome based on RNA-seq profiling. *Plant J* **88**(6): 1058–1070
- Li B, Dong X, Li X, Chen H, Zhang H, Zheng X, Zhang Z (2018) A subunit of the HOPS endocytic tethering complex, FgVps41, is

- important for fungal development and plant infection in *Fusarium graminearum*. *Environ Microbiol* **20**(4): 1436–1451
- Luo KR, Huang NC, Yu TS** (2018) Selective targeting of mobile mRNAs to plasmodesmata for cell-to-cell movement. *Plant Physiol* **177**(2): 604–614
- Marín M, Thallmair V, Ott T** (2012) The intrinsically disordered N-terminal region of AtREM1.3 remorin protein mediates protein-protein interactions. *J Biol Chem* **287**: 39982–39991
- Martín-Hernández AM, Picó B** (2021) Natural resistances to viruses in cucurbits. *Agronomy* **11**(1): 23
- Maule AJ, Palukaitis P** (1991) Virus movement in infected plants. *CRC Crit Rev Plant Sci* **9**(6): 457–473
- Nebenführ A, Gallagher LA, Dunahay TG, Frohlick JA, Mazurkiewicz AM, Meehl JB, Staehelin LA** (1999) Stop-and-go movements of plant Golgi stacks are mediated by the acto-myosin system. *Plant Physiol* **121**(4): 1127–1142
- Niihama M, Takemoto N, Hashiguchi Y, Tasaka M, Morita MT** (2009) ZIP genes encode protein involved in membrane trafficking of the TGN–PVC/Vacuoles. *Plant Cell Physiol* **50**(12): 2057–2068
- Pascual L, Yan J, Pujol M, Monforte AJ, Picó B, Martín-Hernández AM** (2019) CmVPS41 is a general gatekeeper for resistance to *Cucumber Mosaic Virus* phloem entry in melon. *Front Plant Sci* **10**: 1219
- Price A, Seals D, Wickner W, Ungermann C** (2000) The docking stage of yeast vacuole fusion requires the transfer of proteins from a cis-snare complex to a Rab/Ypt protein. *J Cell Biol* **148**(6): 1231–1238
- Rehling P, Darsow T, Katzmann DJ, Emr SD** (1999) Formation of AP-3 transport intermediates requires Vps41 function. *Nat Cell Biol* **1**(6): 346–353
- Reichel C, Beachy RN** (2000) Degradation of tobacco mosaic virus movement protein by the 26S proteasome. *J Virol* **74**(7): 3330–3337
- Roossinck MJ** (2001) *Cucumber mosaic virus*, a model for RNA virus evolution. *Mol Plant Pathol* **2**(2): 59–63
- Sanderson LE, Lanko K, Alsagob M, Almass R, Al-Ahmadi N, Najafi M, Al-Muhaizea MA, Alzaidan H, AlDhalaan H, Perenthaler E, et al.** (2021) Bi-allelic variants in HOPS complex subunit VPS41 cause cerebellar ataxia and abnormal membrane trafficking. *Brain* **144**(3): 769–780
- Schoppe J, Mari M, Yavavli E, Auffarth K, Cabrera M, Walter S, Fröhlich F, Ungermann C** (2020) AP-3 vesicle uncoating occurs after HOPS-dependent vacuole tethering. *EMBO J* **39**(20): e105117
- Serrano I, Buscaill P, Audran C, Pouzet C, Jauneau A, Rivas S** (2016) A non canonical subtilase attenuates the transcriptional activation of defence responses in *Arabidopsis thaliana*. *Elife* **5**: e19755
- Steel D, Zech M, Zhao C, Barwick KES, Burke D, Demailly D, Kumar KR, Zorzi G, Nardocci N, Kaiyrzhanov R, et al.** (2020) Loss-of-function variants in HOPS complex genes VPS16 and VPS41 cause early onset dystonia associated with lysosomal abnormalities. *Ann Neurol* **88**: 867–877
- Su S, Liu Z, Chen C, Zhang Y, Wang X, Zhu L, Miao L, Wang XC, Yuan M** (2010) *Cucumber mosaic virus* movement protein severs actin filaments to increase the plasmodesmal size exclusion limit in tobacco. *Plant Cell* **22**(4): 1373–1387
- Uemura T, Yoshimura SH, Takeyasu K, Sato MH** (2002) Vacuolar membrane dynamics revealed by GFP-AtVam3 fusion protein. *Genes Cells* **7**(7): 743–753
- Vinatzer BA, Teitzel GM, Lee MW, Jelenska J, Hotton S, Fairfax K, Jenrette J, Greenberg JT** (2006) The type III effector repertoire of *Pseudomonas syringae* pv. *syringae* B728a and its role in survival and disease on host and non-host plants. *Mol Microbiol* **62**(1): 26–44
- Vogel F, Hofius D, Sonnewald U** (2007) Intracellular trafficking of potato leafroll virus movement protein in transgenic *Arabidopsis*. *Traffic* **8**(9): 1205–1214